Localized and propagating surface plasmon resonances in aperture-based third harmonic generation

Mohammadreza S. Nezami and Reuven Gordon

December 2015

This article was originally published at:

http://dx.doi.org/10.1364/OE.23.032006

Localized and propagating surface plasmon resonances in aperture-based third harmonic generation

Mohammadreza S. Nezami and Reuven Gordon*

Department of Electrical and Computer Engineering, University of Victoria, Victoria, British Columbia V8P5C2, Canada

*rgordon@uvic.ca

Abstract: We investigate the influence of localized and propagating surface plasmons on third harmonic generation from rectangular apertures in metal films. We designed optimal aperture array structures by using finite-difference time-domain simulations with nonlinear scattering theory. From this design space, we fabricated and measured the third harmonic in the region of maximal performance. We find the highest third harmonic conversion efficiency when the localized resonance is tuned to the fundamental wavelength and the propagating (Bragg) resonance is tuned to the third harmonic; this is 2.5 times larger than the case where the both localized and propagating are tuned to the fundamental wavelength. The two remaining configurations where also investigated with much lower conversion efficiency. When the Bragg resonance is tuned to the third harmonic, directivity improves the collection of third harmonic emission. On the other hand, due to the inherent absorption of gold at the third harmonic, tuning the localized surface plasmon resonance to the third harmonic is less beneficial. All cases showed quantitative agreement with the original theoretical analysis. This work points towards an optimal design criterion for harmonic generation from thin plasmonic metasurfaces.

OCIS codes: (240.6680) Surface plasmons; (190.2620) Harmonic generation and mixing; (160.3918) Metamaterials.

References and links

1. M. Kauranen and A. V. Zayats, "Nonlinear plasmonics," Nat. Photonics **6**(11), 737–748 (2012).
2. A. Nahata, R. A. Linke, T. Ishi, and K. Ohashi, "Enhanced nonlinear optical conversion from a periodically nanostructured metal film," Opt. Lett. **28**(6), 423–425 (2003).
3. C. Min, P. Wang, C. Chen, Y. Deng, Y. Lu, H. Ming, T. Ning, Y. Zhou, and G. Yang, "All-optical switching in subwavelength metallic grating structure containing nonlinear optical materials," Opt. Lett. **33**(8), 869–871 (2008).
4. M. Ren, B. Jia, J.-Y. Ou, E. Plum, J. Zhang, K. F. MacDonald, A. E. Nikolaenko, J. Xu, M. Gu, and N. I. Zheludev, "Nanostructured plasmonic medium for terahertz bandwidth all-Optical switching," Adv. Mater. **23**(46), 5540–5544 (2011).
5. S. Palomba and L. Novotny, "Near-field imaging with a localized nonlinear light source," Nano Lett. **9**(11), 3801–3804 (2009).
6. P.-Y. Chen and A. Alù, "Subwavelength imaging using phase-conjugating nonlinear nanoantenna arrays," Nano Lett. **11**(12), 5514–5518 (2011).
7. T. Thio, H. J. Lezec, T. W. Ebbesen, K. M. Pellerin, G. D. Lewen, A. Nahata, and R. A. Linke, "Giant optical transmission of sub-wavelength apertures: physics and applications," Nanotechnology **13**(3), 429–432 (2002).
8. P. N. Melentiev, T. V. Konstantinova, A. E. Afanasiev, A. A. Kuzin, A. S. Baturin, A. V. Tausenev, A. V. Konyaschenko, and V. I. Balykin, "Single nano-hole as a new effective nonlinear element for third-harmonic generation," Laser Phys. Lett. **10**(7), 075901 (2013).
9. P. N. Melentiev, A. E. Afanasiev, A. A. Kuzin, A. S. Baturin, and V. I. Balykin, "Giant optical nonlinearity of a single plasmonic nanostructure," Opt. Express **21**(12), 13896–13905 (2013).
10. A. Lesuffleur, L. K. S. Kumar, and R. Gordon, "Apex-enhanced second-harmonic generation by using double-hole arrays in a gold film," Phys. Rev. B **75**(4), 045423 (2007).

#251035 Received 28 Sep 2015; revised 26 Nov 2015; accepted 27 Nov 2015; published 3 Dec 2015

11. B. K. Canfield, H. Husu, J. Laukkanen, B. Bai, M. Kuittinen, J. Turunen, and M. Kauranen, "Local field asymmetry drives second-harmonic generation in non-centrosymmetric nanodimers," Nano Lett. **7**(5), 1251–1255 (2007).
12. J. C. Prangsma, D. Oosten, R. J. Moerland, and L. Kuipers, "Increase of group delay and nonlinear effects with hole shape in subwavelength hole arrays," New J. Phys. **12**(1), 013005 (2010).
13. J. A. H. van Nieuwstadt, M. Sandtke, R. H. Harmsen, F. B. Segerink, J. C. Prangsma, S. Enoch, and L. Kuipers, "Strong modification of the nonlinear optical response of metallic subwavelength hole arrays," Phys. Rev. Lett. **97**(14), 146102 (2006).
14. B. L. Wang, R. Wang, R. J. Liu, X. H. Lu, J. Zhao, and Z.-Y. Li, "Origin of shape resonance in second-harmonic generation from metallic nanohole arrays," Sci. Rep. **3**, 2358 (2013).
15. W. Fan, S. Zhang, K. J. Malloy, S. R. J. Brueck, N. C. Panoiu, and R. M. Osgood, "Second harmonic generation from patterned GaAs inside a subwavelength metallic hole array," Opt. Express **14**(21), 9570–9575 (2006).
16. E. H. Barakat, M.-P. Bernal, and F. I. Baida, "Second harmonic generation enhancement by use of annular aperture arrays embedded into silver and filled by Lithium Niobate," Opt. Express **18**(7), 6530–6536 (2010).
17. H. J. Simon, D. E. Mitchell, and J. G. Watson, "Optical second-harmonic generation with surface plasmons in silver films," Phys. Rev. Lett. **33**(26), 1531–1534 (1974).
18. G. S. Agarwal and S. S. Jha, "Theory of second harmonic generation at a metal surface with surface plasmon excitation," Solid State Commun. **41**(6), 499–501 (1982).
19. J. Renger, R. Quidant, N. van Hulst, and L. Novotny, "Surface-enhanced nonlinear four-wave mixing," Phys. Rev. Lett. **104**(4), 046803 (2010).
20. T. Xu, X. Jiao, G. P. Zhang, and S. Blair, "Second-harmonic emission from sub-wavelength apertures: Effects of aperture symmetry and lattice arrangement," Opt. Express **15**(21), 13894–13906 (2007).
21. M. Airola, Y. Liu, and S. Blair, "Second-harmonic generation from an array of sub-wavelength metal apertures," J. Opt. A, Pure Appl. Opt. **7**(2), 118 (2005).
22. K. D. Ko, A. Kumar, K. H. Fung, R. Ambekar, G. L. Liu, N. X. Fang, and K. C. Toussaint, Jr., "Nonlinear optical response from arrays of Au bowtie nanoantennas," Nano Lett. **11**(1), 61–65 (2011).
23. T. Xu, X. Jiao, and S. Blair, "Third-harmonic generation from arrays of sub-wavelength metal apertures," Opt. Express **17**(26), 23582–23588 (2009).
24. S. G. Rodrigo, V. Laliena, and L. Martín-Moreno, "Second-harmonic generation from metallic arrays of rectangular holes," J. Opt. Soc. Am. B **32**(1), 15–25 (2015).
25. R. W. Boyd, *Nonlinear Optics* (Academic Press, 2003).
26. G. Hajisalem, D. K. Hore, and R. Gordon, "Interband transition enhanced third harmonic generation from nanoplasmonic gold," Opt. Mater. Express **5**(10), 2217–2224 (2015).
27. Y. Gong, Z. Li, J. Fu, Y. Chen, G. Wang, H. Lu, L. Wang, and X. Liu, "Highly flexible all-optical metamaterial absorption switching assisted by Kerr-nonlinear effect," Opt. Express **19**(11), 10193–10198 (2011).
28. K. O'Brien, H. Suchowski, J. Rho, A. Salandrino, B. Kante, X. Yin, and X. Zhang, "Predicting nonlinear properties of metamaterials from the linear response," Nat. Mater. **14**(4), 379–383 (2015).
29. S. Roke, M. Bonn, and A. V. Petukhov, "Nonlinear optical scattering: The concept of effective susceptibility," Phys. Rev. B **70**(11), 115106 (2004).
30. A. G. de Beer and S. Roke, "Nonlinear Mie theory for second-harmonic and sum-frequency scattering," Phys. Rev. B **79**(15), 155420 (2009).
31. J. D. Jackson, *Classical Electrodynamics*, 3rd ed. (John Wily and Sons Inc., 1998), 392–394.
32. Y. Chi, G. Chen, F. Jelezko, E. Wu, and H. Zeng, "Enhanced photoluminescence of single-photon emitters in nanodiamonds on a gold film," IEEE Photonics Technol. Lett. **23**(6), 374–376 (2011).
33. V. Knittel, M. P. Fischer, T. de Roo, S. Mecking, A. Leitenstorfer, and D. Brida, "Nonlinear photoluminescence spectrum of single gold nanostructures," ACS Nano **9**(1), 894–900 (2015).
34. F. Przybilla, C. Genet, and T. W. Ebbesen, "Enhanced transmission through Penrose subwavelength hole arrays," Appl. Phys. Lett. **89**(12), 121115 (2006).
35. F. J. García-Vidal, L. Martín-Moreno, E. Moreno, L. K. S. Kumar, and R. Gordon, "Transmission of light through a single rectangular hole in a real metal," Phys. Rev. B **74**(15), 153411 (2006).
36. Z. Ruan and S. Fan, "Superscattering of light from subwavelength nanostructures," Phys. Rev. Lett. **105**(1), 013901 (2010).
37. S. Chen, S. Jin, and R. Gordon, "Super-transmission from a finite subwavelength arrangement of slits in a metal film," Opt. Express **22**(11), 13418–13426 (2014).
38. M. I. Tribelsky and B. S. Luk'yanchuk, "Anomalous light scattering by small particles," Phys. Rev. Lett. **97**(26), 263902 (2006).
39. R. Bardhan, S. Mukherjee, N. A. Mirin, S. D. Levit, P. Nordlander, and N. J. Halas, "Nanosphere-in-a-nanoshell: A simple nanomatryushka," J. Phys. Chem. C **114**(16), 7378–7383 (2010).
40. A. E. Miroshnichenko, "Non-Rayleigh limit of the Lorenz-Mie solution and suppression of scattering by spheres of negative refractive index," Phys. Rev. A **80**(1), 013808 (2009).
41. J. A. Schuller, T. Taubner, and M. L. Brongersma, "Optical antenna thermal emitters," Nat. Photonics **3**(11), 658–661 (2009).
42. J. Aizpurua, P. Hanarp, D. S. Sutherland, M. Käll, G. W. Bryant, and F. J. García de Abajo, "Optical properties of gold nanorings," Phys. Rev. Lett. **90**(5), 057401 (2003).

#251035 Received 28 Sep 2015; revised 26 Nov 2015; accepted 27 Nov 2015; published 3 Dec 2015

43. M. W. Klein, M. Wegener, N. Feth, and S. Linden, "Experiments on second- and third-harmonic generation from magnetic metamaterials," Opt. Express **15**(8), 5238–5247 (2007).
44. N. Kalhor, S. A. Boden, and H. Mizuta, "Sub-10 nm patterning by focused He-ion beam milling for fabrication of downscaled graphene nano devices," Microelectron. Eng. **114**, 70–77 (2014).
45. X. Chen, C. Ciracì, D. R. Smith, and S. H. Oh, "Nanogap-enhanced infrared spectroscopy with template-stripped wafer-scale arrays of buried plasmonic cavities," Nano Lett. **15**(1), 107–113 (2015).
46. W. Zhu, M. G. Banaee, D. Wang, Y. Chu, and K. B. Crozier, "Lithographically fabricated optical antennas with gaps well below 10 nm," Small **7**(13), 1761–1766 (2011).
47. R. Stosch, F. Yaghobian, T. Weimann, R. J. C. Brown, M. J. T. Milton, and B. Güttler, "Lithographical gap-size engineered nanoarrays for surface-enhanced Raman probing of biomarkers," Nanotechnology **22**(10), 105303 (2011).
48. A. Zehtabi-Oskuie, A. A. Zinck, R. M. Gelfand, and R. Gordon, "Template stripped double nanohole in a gold film for nano-optical tweezers," Nanotechnology **25**(49), 495301 (2014).

1. Introduction

Metasurfaces are of interest for nonlinear optics to achieve functionality in a thin layer, for applications including wavelength conversion [1,2], switching [1,3,4] and near-field light sources (imaging) [5,6]. Among these surfaces, aperture-based structures in metal films are particularly promising because they efficiently remove heat and localize the electromagnetic field [7–9]. A key challenge is to create structures for high conversion efficiency.

Past works on plasmonic enhanced nonlinear conversion have optimized the localized surface plasmon (LSP) using different aperture and particle shapes, as well as the surrounding media [10–16]. Furthermore, Bragg resonances of propagating surface plasmon polaritons (SPPs) were also optimized to attain highest conversion efficiency [17–19]. A few works have investigated both LSP and SPP resonances at the fundamental or harmonic wavelength on nonlinear optical response of metasurfaces [20–24]. However, there is still a question about what combination of LSP and SPP should be used to achieve the greatest conversion efficiency.

Here we investigate the optimal combination of LSP and SPP resonances to maximize conversion efficiency in third harmonic generation (THG) from nanoapertures in a gold film. We explore all combinations where the fundamental and harmonic wavelengths are enhanced by the LSP and/or SPP resonance conditions, finding the greatest enhancement when the fundamental is at the LSP resonance and the harmonic is at the SPP resonance. Here we focus on THG for four main reasons. The centrosymmetry of gold means SHG is dipole-forbidden in the bulk [25]. On a related point, the cubed dependence of THG may enable higher conversion efficiencies at increased power levels (as opposed to SHG which has a squared dependence) [25]. Gold has an interband resonance in THG near the fundamental of ~1400-1600 nm, so that low-cost, high-power fiber-based lasers may be used as sources for compact wavelength conversion [26]. The $\chi^{(3)}$ susceptibility of THG also allows for Kerr-like switching, so this may be of interest to future switching applications [27]. Our experimental results agree well with nonlinear scattering theory using finite-difference time-domain (FDTD) simulations.

2. Nonlinear Scattering Theory

We performed a theoretical analysis using FDTD simulations (Lumerical FDTD 8.12.501) to guide our experiments. The nonlinear scattering theory approach is similar to a recent work looking at U-shaped nanoparticles to optimize SHG [28]; however, here it is configured for THG and for apertures. In particular, we consider the local field intensity for the fundamental and harmonic wavelengths for the configuration shown in Fig. 1(a). We use reciprocity to calculate the conversion efficiency, where the harmonic beam is incident from the opposite side (and we employ time-reversal symmetry in scattering theory to relate this to the generated field that leaves the aperture array [29,30]). Then we integrate the overlap of the field intensities (of each contributing photon) over the gold volume to estimate the THG using the equation:

#251035 Received 28 Sep 2015; revised 26 Nov 2015; accepted 27 Nov 2015; published 3 Dec 2015

$$THG \propto \int_{gold} E_{3\omega} \times E_{\omega}^{3} dV \tag{1}$$

Where $E_{3\omega}$ is the electric field of the third harmonic and E_{ω} is the electric field of the fundamental light. This equation shows physically that the fundamental beam creates a nonlinear current source with amplitude $J \propto E_{\omega}^{3}$, and this couples into the third harmonic beam with field $E_{3\omega}$. By Lorentz reciprocity, the outcoupling goes as $J \cdot E_{3\omega}$ integrated over the volume of the source [31]. The third harmonic beam is solved by considering a plane wave incident on the aperture array; however, this gives the same coupling intensity to the outgoing wave by reciprocity. Using this integral relation, we can search over four parameter spaces where the SPP and LSP are optimized for combinations of the fundamental and harmonic wavelengths.

While the LSP resonance can be controlled by the dimensions of the aperture in the array, the SPP resonance is tuned by changing the periodicity of the array. Figure 1(c) shows the resultant THG using Eq. (1) for LSP resonance at the harmonic wavelength (523 nm) and SPP resonance at the fundamental wavelength (1570 nm) where l is the length of the rectangular aperture and P_y is the periodicity of the rectangular array in y direction. The width of the aperture, w, and the periodicity of the array, P_x, were fixed at 30 nm and 1400 nm. Figure 1(d) shows the same results for LSP and SPP resonances at the third harmonic wavelength. Figure 1(e) shows the calculated THG for LSP and SPP resonances at the fundamental wavelength and Fig. 1(f) shows the results for LSP resonance at the fundamental wavelength and the SPP resonance at the third harmonic wavelength. These are plotted on a natural log-scale. From these simulations, we obtained a region of interest for fabrication for each scenario to give the best conversion efficiency. The actual fabricated dimensions are shown with the black dots on Figs. 1(c)-(f).

#251035 Received 28 Sep 2015; revised 26 Nov 2015; accepted 27 Nov 2015; published 3 Dec 2015

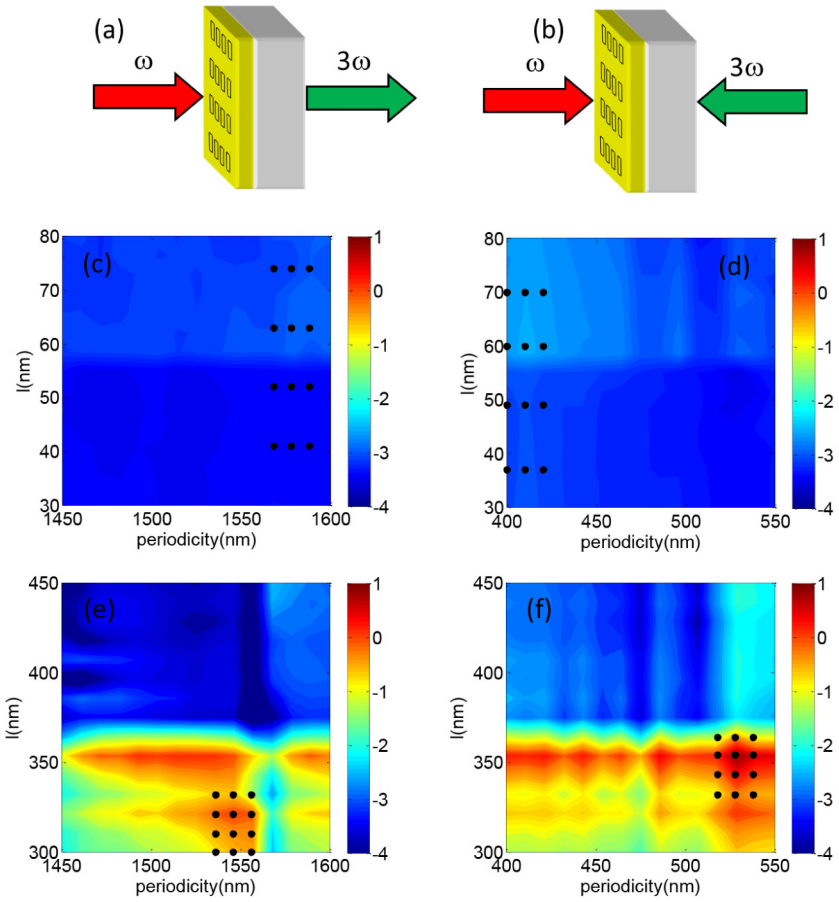

Fig. 1. (a) Schematic of third harmonic generation from a rectangular aperture array. (b) Simulated configuration for incident fundamental and third harmonic waves (using time-reversal for the harmonic beam). (c) Calculated THG in natural logarithm scale using nonlinear scattering theory of Eq. (1) for LSP resonance at 523 nm and SPP resonance at 1570 nm. (d) Same as (c) for LSP and SPP resonance at 523 nm. (e) Same as (c) for LSP and SPP resonance at 1570 nm. (f) Same as (c) for LSP resonance at 1570 nm and SPP resonance at 523 nm. Black dots show fabricated dimensions.

3. Fabrication and THG measurement

Guided by the simulation results, we fabricated the nanostructures around the maxima shown in Fig. 1. Focused ion beam (FIB) milling was used to fabricate the arrays of rectangles. A Ga ion beam was focused on a spot of 15 μm of 100 nm thick gold film at 40 KV acceleration voltage, 0.01064 nA beam current and dwell time of 10 μs.

Figure 2 shows scanning electron microscope images of the fabricated structures for different periodicities in y direction (P_y) and length of rectangle (l) corresponding to different LSP and SPP resonances. The periodicity in x direction (P_x) and width of rectangle (w) took fixed values of 1400 nm and 30 nm.

Figure 3(a) shows a schematic of the THG measurements. We have used a 100 fs pulsed laser at 1570 nm with 40 MHz repetition rate. The incident power was 40 mW, focused onto the sample by an objective lens (40 × , NA = 0.65). Theoretically, the spot size should be approximately 3 microns based on the wavelength and objective used, which is close to the size of the array (7.3 micron side). In practice, we found that the focusing was sensitive to translations around 10 microns (smoothly varying over this range), so the spot size is likely

#251035 Received 28 Sep 2015; revised 26 Nov 2015; accepted 27 Nov 2015; published 3 Dec 2015

slightly larger than the array. A guide laser beam at the wavelength of 853 nm was used to help alignment, but was turned off during the measurements. The third harmonic beam on the transmission side was collected by a second objective lens (40 × , NA = 0.65).

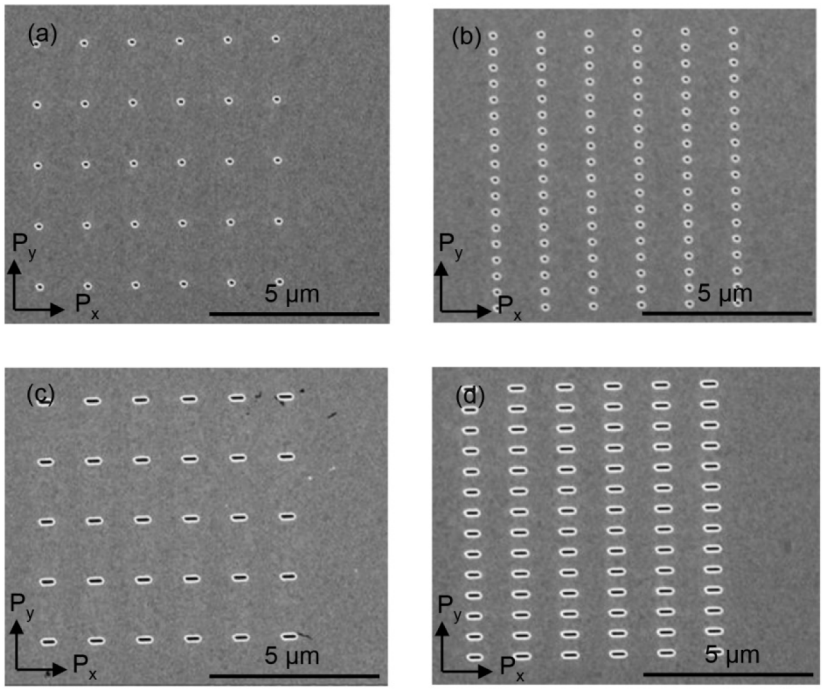

Fig. 2. Scanning electron microscopy images of the fabricated structures on a 100 nm thick gold film for: (a) LSP resonance at 523 nm and SPP resonance at 1570 nm (l = 41 nm, Py = 1578 nm). (b) LSP resonance at 523 nm and SPP resonance at 523 nm (l = 70 nm, Py = 400 nm). (c) LSP resonance at 1570 nm and SPP resonance at 1570 nm (l = 310 nm, Py = 1546 nm). (d) LSP resonance at 1570 nm and SPP resonance at 523 nm (l = 343 nm, Py = 528 nm). Where l is the length of the rectangular aperture and P_y is the periodicity of the array in y direction. The width of the aperture (w) and the periodicity of the array in x direction (P_x) were fixed values of 30 nm and 1400 nm.

We confirmed that the transmitted beam contained THG by the power scaling of the light at the spectrometer (Fig. 3(b)) and by the wavelength of the emitted light (Fig. 3(c)). The fundamental beam was not detected by the photodiode. Bright green emission was visible on a CMOS camera (Thorlabs, DCC1545M), as shown in Fig. 3(d). There is photoluminescence [32,33] present in the measurements, however, this is much weaker than the third harmonic and consequently not visible in Fig. 3(c). To estimate the directivity of the THG, we removed the collection objective and placed an iris in the beam 3 cm from the gold surface. The THG collected reduced when the iris was reduced to 1 mm, implying a half angle of approximately 1°. Theoretically, the angle from a Gaussian aperture of 7.3 microns (width of the array) at 523 nm should be 1.3°.

Figure 4 shows the final result of this work, comparing the THG for different configurations of SPP and LSP resonances at the fundamental and the third harmonic wavelengths. Good agreement is seen between the simulation results using the reciprocity relation in Eq. (1) and the experiment. Note, the entire experiment was repeated to ensure reproducibility of the results.

#251035 Received 28 Sep 2015; revised 26 Nov 2015; accepted 27 Nov 2015; published 3 Dec 2015

4. Discussion

Here we discuss the key features found for efficient THG from the simulations and experiments. First, it is advantageous to tune the SPP resonance (i.e., the Bragg resonance of the periodic hole spacing) to the third harmonic wavelength instead of the fundamental wavelength. This is seen for both LSP configurations. The reason for this is related to the requirement to efficiently out-couple the THG away from the aperture array and towards the detector. The Bragg resonance improves the out-coupling efficiency of the third harmonic by directively coupling it to an out-going plane wave. While nonlinear interactions can be boosted by tuning the Bragg resonance of the lattice to the third harmonic, the directivity of the third harmonic signal is also improved. The latter helps to efficiently out-couple third harmonic signal towards the detector and consequently prevents the resonant absorption of THG at the gold surface.

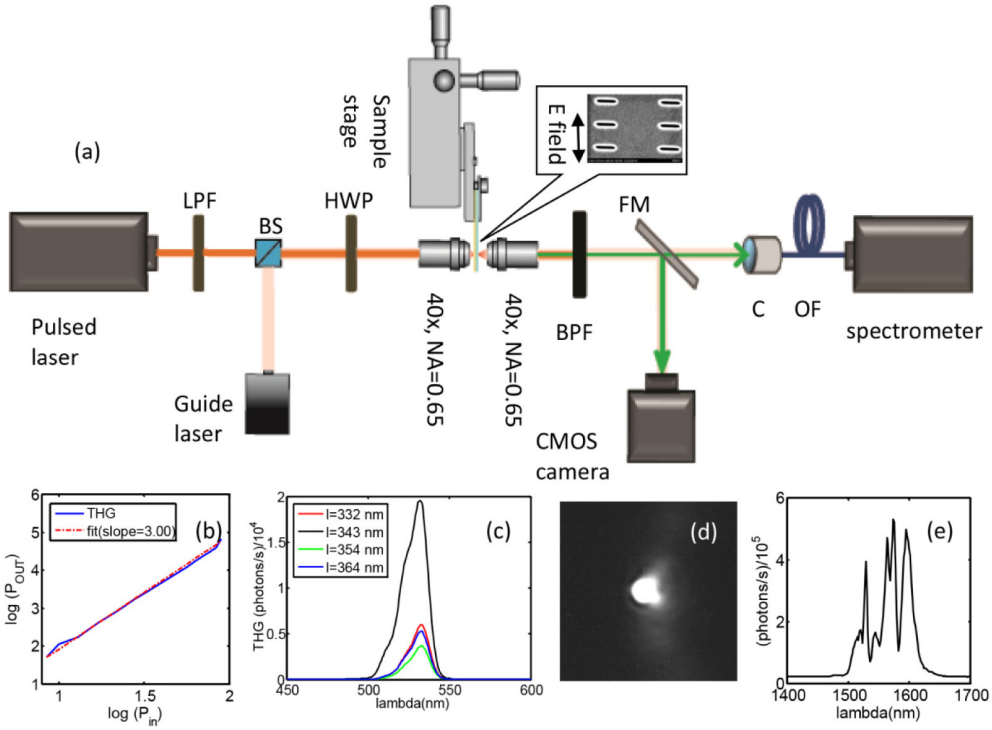

Fig. 3. (a) Schematic of the experimental setup used to measure THG of the fabricated array of rectangles where LPF is low pass filter, BS is beam splitter, HWP is half wave plate, FM is flip mirror, C is collimator and OF is optical fiber. The inset shows the sample with the electric field polarization of the incident beam. (b) Power dependence of measured THG (solid blue curve) on the input power in logarithm scale. The dashed red curve shows a fit with slope 3. (c) Measured THG for the array designed for LSP resonance at 1570 nm and SPP resonance at 523 nm that yields the maximum conversion efficiency for different length of the aperture and fixed P_y = 518 nm. (d) Third harmonic green spot imaged on the CCD camera. (e) measured power spectrum of the pulsed laser source.

Next we note that it is best to have the LSP resonance of the aperture at the fundamental wavelength. The LSP resonance provides a strong local field at the aperture, which gives an increased THG when considering Eq. (1) (since the THG scales as the cube of the fundamental intensity). Of course, it is possible to obtain high field intensity by using the SPP Bragg (grating) resonance as well, and indeed, the second best efficiency results are obtained when both the LSP and SPP are at the fundamental wavelength. However, this comes at the expense of efficient directive outcoupling of the THG, and so it did not yield the greatest

#251035 Received 28 Sep 2015; revised 26 Nov 2015; accepted 27 Nov 2015; published 3 Dec 2015

THG detected. In other words, in this case the LSP resonance of the apertures is tuned to the fundamental wavelength, which results in efficient confinement of the incident beam. The Bragg resonance can also improve nonlinear interactions inside the apertures further due to an improved in-coupling. However, the TH signal is not efficiently out-coupled in this case and so the overall THG collected is reduced.

Past works on aperture arrays show that the Bragg resonance saturates for over 100 apertures for circular holes in a square array [34]. Here, the saturation is expected to be faster because we are using rectangular apertures. Indeed, in the simulated spectra (which assume infinite arrays and plane wave excitation) the full-width at half-maximum is 72 nm at the fundamental wavelength. Therefore, the quality factor of the resonances is about 20, which means that the light will couple over approximately 20 periods before being mostly scattered. This is below the size of the aperture arrays used (15 periods in the direction of polarization) and so we believe that we have not saturated the coupling, but we are close to that limit.

Interestingly, it does not seem particularly advantageous to put the LSP at the third harmonic wavelength. While the resonance at the third harmonic will enhance the THG from Eq. (1), it does so only with a linear power. Furthermore, the LSP at the third harmonic leads to local resonant absorption by the gold, so that much of the light will not be detected.

Related to this point, it should be noted that the LSP resonance is very effective at coupling the incident light into the aperture, and so there is little benefit from adding the

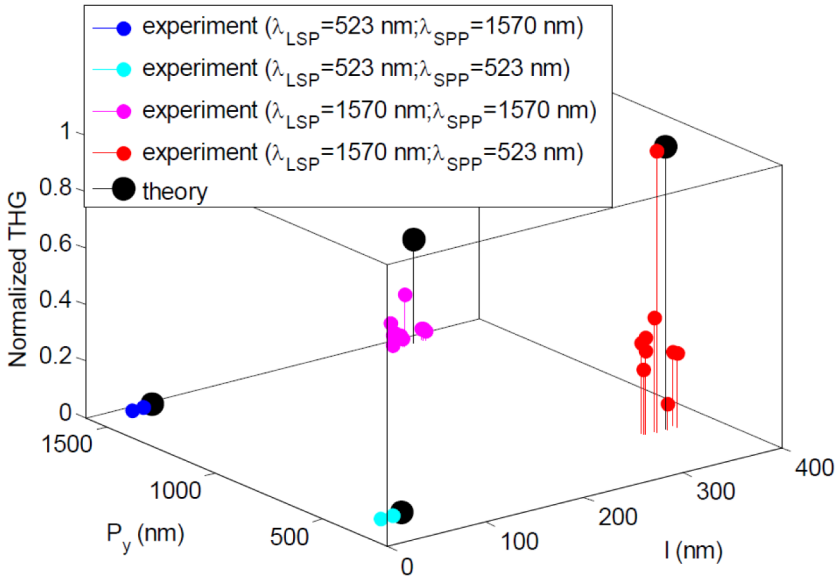

Fig. 4. Normalized third harmonic generation versus array parameters for different LSP and SPP resonance scenarios. Theoretical results from simulations are also shown.

SPP Bragg resonance. For example, it has been shown that the normalized transmission through an aperture at the LSP resonance is close to a quarter of the wavelength squared [35]. When we consider the aperture as a dipole that radiates in the forward and backward directions equally, the total scattering of that aperture is already close to the single channel limit [36,37]. This should be compared with particle plasmonics, where the scattering cross section is usually less than a third of the single channel limit [38–42]. In summary, rectangular apertures have a very strong LSP resonance that benefits THG.

From our experiments, we measure an output power at 523 nm by replacing the spectrometer with an avalanche photodiode (Thorlabs – APD 110A). Using the responsivity specified for this APD at 523 nm (measuring 30 mV for the maximum THG), we estimate that The maximum achieved total conversion efficiency of the aperture array (including all

#251035 Received 28 Sep 2015; revised 26 Nov 2015; accepted 27 Nov 2015; published 3 Dec 2015

collection optics) is 0.05%. The green light is clearly observable by bare eyes. For comparison, the conversion efficiency for a split ring resonator array was reported to be $3 \times 10^{-5\%}$ [43], and the conversion efficiency for a single aperture was reported to be 0.001% [9]. Even though we are still far away from ~10% percent conversion efficiencies, there are some avenues that could lead us to get closer to that goal. Using apertures prevents the sample from overheating by having a good conducting layer [8,9]. Therefore, we can benefit from a higher power pulsed laser to boost conversion efficiency without suffering from melting (estimated to be 3 orders of magnitude lower heating than for comparable plasmonic particles [9]). Moreover, confining light in a very small gap can increase the power further and contribute to increased THG. By using new fabrication techniques such as He beam milling [44], atomic layer deposition (ALD) [45], shadow mask [46,47] and template stripping [48], a gap size below 10 nm should be achievable.

5. Conclusions

We have investigated the third harmonic generation from rectangular aperture arrays in a metal film and found that the maximum conversion efficiency occurs when the localized surface plasmon resonance of the aperture is tuned the fundamental wavelength and the propagating surface plasmon resonance is tuned to the third harmonic wavelength. Directivity improves the outcoupling of the third harmonic at the Bragg resonance. We also investigated the other cases where the LSP and SPP are tuned to the fundamental and/or third harmonic. We found that tuning the LSP resonance to the third harmonic wavelength is not that advantageous since it leads to resonant absorption.

Acknowledgements

MSN would like to thank Ghazal Hajisalem, Wei Su, Ryan Gelfend, Afshin Jooshesh, Abhay Kotnala and Ahmed A. Al Balushi for valuable discussions. Funding was provided by the NSERC Discovery Grants program.